Separating the shortwave and longwave components of greenhouse gas radiative forcing

Shine, K. P. ORCID: https://orcid.org/0000-0003-2672-9978, Byrom, R. E. ORCID: https://orcid.org/0000-0002-5992-6962 and Checa-Garcia, R. ORCID: https://orcid.org/0000-0001-7653-3653 (2022) Separating the shortwave and longwave components of greenhouse gas radiative forcing. Atmospheric Science Letters, 23 (10). e1116. ISSN 1530-261X doi: 10.1002/asl.1116 Available at https://centaur.reading.ac.uk/105665/

Received: 25 January 2022 | Revised: 31 March 2022 | Accepted: 25 May 2022

DOI: 10.1002/asl.1116

RESEARCH ARTICLE

Atmospheric Science Letters RMetS

Separating the shortwave and longwave components of greenhouse gas radiative forcing

Keith P. Shine[1] | **Rachael E. Byrom**[1,2] | **Ramiro Checa-Garcia**[3]

[1]Department of Meteorology, University of Reading, Reading, UK

[2]CICERO Center for International Climate Research, Oslo, Norway

[3]Institute of Meteorology and Climatology, University of Natural Resources and Life Sciences, Vienna, Austria

Correspondence
Keith P. Shine, Department of Meteorology, University of Reading, Earley Gate, Reading RG6 6ET, UK.
Email: k.p.shine@reading.ac.uk

Funding information
Natural Environment Research Council, Grant/Award Number: SCENARIO Doctoral Training Partnership

Abstract

Many important greenhouse gases (including water vapour, carbon dioxide, methane and ozone) absorb solar radiation. When gas concentrations change, this absorption exerts a radiative forcing that modifies the thermal infrared ('longwave') radiative forcing which is predominant for most gases (ozone being a major exception). The nature of the solar forcing differs from the longwave forcing in several ways. For example, the sign of the instantaneous solar forcing can differ between the tropopause and top-of-atmosphere, and the sign can differ between gases. In addition, a significant part of the solar forcing can be manifested in the longwave, following stratospheric temperature adjustment, which can counteract or enhance the instantaneous solar forcing. Here the nature of solar forcing is examined via a mixture of idealised and more realistic calculations, which consider the effect of perturbations in carbon dioxide, methane and ozone. An apparent contradiction in the sign of the solar forcing of carbon dioxide is resolved; it is shown to be negative, reducing the net carbon dioxide forcing by about 2.3%. The relevance of this work to the effective radiative forcing concept is also discussed.

KEYWORDS

carbon dioxide, methane, ozone, radiative forcing, solar radiation

1 | INTRODUCTION

As well as absorbing thermal infrared radiation ('longwave [LW]' hereafter), greenhouse gases (hereafter GHGs, including H_2O, CO_2, O_3 and CH_4) absorb incoming solar radiation at near-infrared and sometimes visible and ultra-violet wavelengths (e.g., Gordon et al., 2017). We refer to this as shortwave (SW), often taken to be wavelengths less than 4 μm, acknowledging that some solar radiation is incident at longer wavelengths.

Many papers consider GHG LW radiative forcing in detail (e.g., Ramaswamy et al., 2018) and several explore mechanisms by which this forcing is manifested; Dufresne et al. (2020) presented an elegant demonstration of the relative contributions of increased atmospheric opacity, and the related change in emission height to CO_2 forcing. However, while GHG shortwave absorption, especially by H_2O, CO_2 and O_3, has long been included in climate model calculations (e.g., Manabe & Wetherald, 1967), its radiative forcing role has been relatively neglected, with the exception of O_3. In addition, the radiative forcing literature indicates apparent contradictions in the sign of the SW forcing. An intercomparison of climate model radiative transfer codes (Collins et al., 2006) demonstrated that, at that time,

many ignored GHG SW absorption beyond those mentioned above; Pincus et al. (2020) report progress in recent years.

This letter aims to resolve apparent contradictions in the nature of SW GHG radiative forcing. After reviewing current understanding, idealised and more realistic model calculations illustrate the SW processes in the framework of the instantaneous radiative forcing (IRF) and radiative forcing including stratospheric temperature adjustment (henceforth RF) (e.g., Myhre et al., 2013). The relevance to Effective Radiative Forcing (ERF) (e.g., Myhre et al., 2013) is also discussed.

2 | CURRENT UNDERSTANDING

Hansen et al. (1981) presented calculations of top-of-atmosphere (TOA) LW and SW forcing due to a CO_2 doubling from 300 ppm. IRF_{SW} was 0.1 $W{\cdot}m^{-2}$, compared to IRF_{LW} of 2.4 $W{\cdot}m^{-2}$. The TOA RF_{SW} (i.e., forcing including stratospheric temperature adjustment) of 0.1 $W{\cdot}m^{-2}$ is unchanged from its IRF value; RF_{LW} is 3.8 $W{\cdot}m^{-2}$, significantly higher than IRF_{LW}. Hence, Hansen et al. (1981) found a *positive* SW forcing of 2.6% or 4% of the net (LW + SW) forcing, depending on whether RF or IRF is considered. The view that CO_2 IRF_{SW} is positive re-emerged in the ERF framework, which takes a TOA perspective (e.g., fig. 14-6 of Ramaswamy et al., 2018).

By contrast, Cess et al. (1993) reported that CO_2 IRF_{SW} was *negative*, and about 6% of IRF_{LW} (for a doubling from 330 ppm). This view became established, although not all studies have found a negative CO_2 tropopause IRF_{SW} (Forster et al., 2001). The apparent contradiction is because Cess et al. (1993) defined forcing at the tropopause; Hansen et al. (1981) chose TOA. This still leaves a question as to which perspective is of most value, and whether they can be reconciled.

Myhre et al. (1998) also found a negative IRF_{SW} for CO_2 of order 4% (−0.11 $W{\cdot}m^{-2}$) of RF_{LW}, for a doubling from 278 ppm. However, and of importance here, the additional SW absorption warms the stratosphere (relative to the LW-only case). In the RF framework, Myhre et al. (1998) calculated that this warming led to a positive tropopause RF_{LW} (0.05 $W{\cdot}m^{-2}$); thus, the net RF due to SW forcing (−0.06 $W{\cdot}m^{-2}$) is about half IRF_{SW}.

For increased concentrations of stratospheric H_2O, Forster and Shine (2002) (see also Forster et al., 2001; Myhre et al., 2007, 2009) found a negative tropopause IRF_{SW}, offsetting about 20% of RF_{LW}.

Etminan et al. (2016) presented IRF_{SW} calculations for methane; the tropopause IRF_{SW} (for a 750–1800 ppb perturbation) was positive and 6% of the total forcing; accounting for the effect of warming of the stratosphere due to the additional SW absorption on RF_{LW}, methane's SW forcing enhanced the LW-only RF by 15%.

Ozone is a distinct GHG because of its strong absorption of ultraviolet (and, to some extent, visible) radiation. Its SW forcing has long been recognised (e.g., Ramaswamy et al., 1992; Ramaswamy and Bowen, 1994; Hauglustaine et al., 1994) but, to our knowledge, the specific role of SW absorption in modifying RF_{LW} has not been isolated. The differing TOA and tropopause perspectives have been indicated, but not fully explained, by Michou et al. (2020); they found the signs of TOA ERF_{SW} and ERF_{LW} for stratospheric ozone depletion were opposite to the tropopause RF_{LW} and RF_{SW} calculations of Checa-Garcia et al. (2018).

Taken together, these studies show that the apparent SW forcing depends on whether a tropopause or TOA perspective is taken, and whether its impact on stratospheric temperature adjustment (and hence on RF_{LW}) is accounted for. They also show that the sign of SW forcing varies among gases, sometimes enhancing and sometimes opposing RF_{LW}. This letter constructs a framework to better understand SW forcing and to resolve apparent contradictions. This stresses that judging the importance of SW forcing via IRF_{SW}, RF_{SW} or ERF_{SW} alone gives a misleading impression.

The impact of SW forcing on the LW via stratospheric temperatures (in the RF framework) and rapid (tropospheric and stratospheric) temperature adjustments (in the ERF framework) must be accounted for to give a correct impression of the size and sometimes the sign of SW forcing. In the ERF framework, other adjustments (e.g., in clouds and water vapour) driven by SW processes can also impact on ERF_{LW}; similarly, changes driven by LW processes can impact on ERF_{SW} (e.g., Donohoe et al., 2014).

TOA IRF_{SW} must be positive (consistent with Hansen et al. (1981)) for GHG concentration increases. Additional shortwave absorption always decreases planetary albedo. At the tropopause, the situation is unclear, unless the gas perturbation is solely in the stratosphere. Stratospheric absorption deprives the troposphere of radiation giving a negative IRF_{SW}. However, additional tropospheric absorption decreases the albedo of the troposphere-surface system giving a positive IRF_{SW}. Hence the tropopause IRF_{SW} can have either sign.

Etminan et al. (2016) show that the sign of CO_2 and CH_4 tropopause IRF_{SW} varies with wavelength. They also show that the sign depends on the intensity of absorption features (for strong absorption features, additional absorption is mostly in the stratosphere, leading to a negative IRF_{SW}), and overlap with strong near-IR water vapour bands; if these bands are saturated in the troposphere, additional absorbers exert little influence on the upwelling irradiance at the tropopause. By contrast,

additional absorption in relatively transparent windows between these bands can lead to a positive IRF_{SW}. This is especially so for cloudy skies, as tropospheric albedo is higher, and the importance of absorption of upwelling radiation by the gas is enhanced; Etminan et al. (2016) find the wavelength-integrated CH_4 IRF_{SW} at the tropopause is negative for clear skies but positive when clouds are included (although Collins et al., 2018 found it to be positive in both cases). Etminan et al. (2016) found it was negative in both cases for CO_2.

As noted above, IRF alone cannot constrain the effect of shortwave absorption; within the RF framework, the impact of increased stratospheric SW absorption on LW forcing must be considered. Section 3 uses idealised calculations to illustrate this.

3 | IDEALISED CALCULATIONS WITH NO INSTANTANEOUS LONGWAVE RADIATIVE FORCING

The idealised calculations of SW forcing employ the LW code of Shine and Myhre (2020) and the SW code of Slingo and Schrecker (1982) with updated gaseous absorption coefficients from Chagas et al. (2001). Calculations use a global-mean atmospheric profile (temperature, humidity, ozone and clouds) from Freckleton et al. (1998) with a global-mean tropopause of 128.6 hPa, global-mean insolation (solar zenith angle of 60° for 12 h) and a spectrally-constant surface albedo of 0.06 (representing a sea surface). The forcing due to a grey absorber which is added only to near-IR bands (wavelengths greater than 1 μm) is computed; that is, there is no IRF_{LW}. The grey absorber has an absorption coefficient of 4×10^{-4} $m^2 \cdot kg^{-1}$ and a constant mass mixing ratio of 0.0005 $kg \cdot kg^{-1}$, giving an optical depth of 0.003 when the absorber is in the stratosphere only and 0.024 when at all altitudes. RF is computed by a standard time-stepping procedure that adjusts stratospheric temperature until the LW + SW heating rates return to global-mean radiative equilibrium.

In Idealised Example 1 (Table 1), the grey absorber is in the stratosphere only. As expected from Section 2, IRF_{SW} is positive at TOA, and negative at the tropopause. This causes additional stratospheric absorption of solar radiation; in this case, the TOA forcing is +0.29 $W \cdot m^{-2}$, the tropopause forcing is −0.54 $W \cdot m^{-2}$, giving a convergence of 0.83 $W \cdot m^{-2}$. The consequent warming of the stratosphere increases LW emission to space and the troposphere. Increased upward TOA irradiance constitutes a negative LW forcing; increased downward tropopause irradiance constitutes a positive LW forcing. Thus, RF_{LW} is opposite in sign and comparable in size to IRF_{SW} at both TOA and tropopause (Table 1).

It is initially surprising that at TOA, RF_{LW} (−0.4 $W \cdot m^{-2}$) is larger in magnitude than IRF_{SW}. However, increased LW emission from the stratosphere due to the adjustment (0.4 $W \cdot m^{-2}$ upwards at TOA and 0.43 $W \cdot m^{-2}$ downwards at the tropopause) is consistent, as it should be, with the 0.83 $W \cdot m^{-2}$ convergence of SW radiation. In this case, RF_{LW} is nearly equal at TOA and tropopause; the SW effect on RF_{LW} could be estimated by partitioning the convergence of SW radiation in this way. This is because the grey absorber is at all stratospheric levels. When placed in the topmost layer only (at 1 hPa), TOA RF_{LW} is about 6 times larger than the tropopause RF_{LW}. When placed only in the layer closest to the tropopause, the tropopause RF_{LW} is about double TOA RF_{LW}.

The net forcing, RF_{NET}, at TOA and tropopause is now equal (−0.11 $W \cdot m^{-2}$), as is required following stratospheric temperature adjustment. In this example, because SW absorption deprives the surface-troposphere system of energy, RF_{NET} is negative but, because of the compensatory effect of increased stratospheric LW emission, it is only 20% of the value inferred from the tropopause IRF_{SW}.

This illustrates how IRF_{SW} differs in sign between the TOA and tropopause perspectives (i.e., there is no contradiction in the literature) and also illustrates how SW absorption cannot be judged from IRF_{SW} alone; the effect on RF_{LW} must be considered. Once RF_{LW} is included, there is no ambiguity in the sign of RF_{NET} and it agrees at TOA and tropopause.

In Idealised Example 2 (Table 2) the grey absorber is present at all altitudes. IRF_{SW} is now positive at both TOA and tropopause, because of increased tropospheric absorption of solar radiation. Because stratospheric convergence of SW radiation is only slightly affected by

TABLE 1 Idealised example 1: Global and annual instantaneous and adjusted radiative forcing ($W \cdot m^{-2}$) at the top-of-atmosphere and tropopause when including a weakly-absorbing grey shortwave-only absorber in the stratosphere only

	Instantaneous			Adjusted		
$W\ m^{-2}$	LW	SW	Net	LW	SW	Net
TOA	0.0	+0.29	+0.29	−0.40	+0.29	−0.11
Tropopause	0.0	−0.54	−0.54	+0.43	−0.54	−0.11

TABLE 2 Idealised example 2: Global and annual instantaneous and adjusted radiative forcing ($W \cdot m^{-2}$) at the top-of-atmosphere and tropopause when including a weakly-absorbing shortwave-only grey absorber at all altitudes

	Instantaneous			Adjusted		
$W \cdot m^{-2}$	LW	SW	Net	LW	SW	Net
TOA	0.0	+1.50	+1.50	−0.39	+1.50	+1.11
Tropopause	0.0	+0.67	+0.67	+0.43	+0.67	+1.11

tropospheric absorption (i.e., 1.50–0.67 = 0.83 $W \cdot m^{-2}$ as in Example 1), RF_{LW} from stratospheric temperature adjustment is almost identical to Table 1. In this case, RF_{LW} is a smaller proportion of IRF_{SW}, and RF_{NET} is positive.

Again, this example illustrates that forcing due shortwave absorption cannot be judged by IRF_{SW} alone, although in this case the sign of IRF_{SW} is the same at TOA and tropopause and consistent with RF_{NET}.

4 | MORE REALISTIC CALCULATIONS FOR CARBON DIOXIDE, METHANE AND OZONE

The role of SW forcing in more realistic cases is calculated using the more sophisticated configuration of Checa-Garcia et al. (2018). RF is calculated on a 5° × 5° horizontal grid; stratospheric temperature adjustment is calculated using the fixed-dynamical heating method. It uses the SOCRATES radiative transfer code (Walters et al., 2019), using the Met Office Earth System Model configuration: 9 LW bands (wavenumbers 1–2995 cm^{-1}) and 6 SW bands (wavenumbers 1–50,000 cm^{-1}). Unlike Section 3, IRF has both LW and SW components. We perform calculations with both LW and SW components, and then repeat them with only the LW component active ('LW only' in the tables). The difference between these yields the total RF_{SW} forcing, including its impact on RF_{LW} via stratospheric temperature adjustment.

SOCRATES is regularly updated to reflect its performance in radiation code intercomparisons (e.g., Pincus et al., 2015) and updated spectral data. Walters et al. (2019) (their sec. 3.2.1) document significant improvements in the version used here, relative to a high-spectral resolution code which was compared with other benchmark codes in Pincus et al. (2020).

The example GHGs (CO_2, CH_4, O_3) are the ones most widely discussed in earlier work (Section 2); their different behaviours should guide how other GHGs would behave. CO_2 has intense SW stratospheric absorption so that its tropopause IRF_{SW} is negative; methane is weaker giving a positive tropopause IRF_{SW}; ozone is unusual as RF_{SW} and RF_{LW} are comparable. Etminan et al. (2016) demonstrate that nitrous oxide's RF_{SW} is much smaller than gases considered here. The results presented here are highly relevant to the ERF framework. Stratospheric temperature adjustment is the largest adjustment in ERF calculations for CO_2 (Smith et al., 2018) and ozone (Skeie et al., 2020); for methane, adjustments are small when RF_{SW} is neglected, but are more important when it is included (Etminan et al., 2016).

Calculations use multi-year (2000–2009) monthly-mean averages of temperature, water vapour, clouds and surface albedo from ERA-Interim (Checa-Garcia et al., 2018). The source of ozone fields is described below. Calculations include the impact of tropospheric scattering of solar radiation by clouds and the surface on absorption of SW radiation in the stratosphere; this has been shown (Section 2) to be important in quantifying methane's IRF_{SW} (Collins et al., 2018; Etminan et al., 2016). To demonstrate the role of SW forcing, methane and CO_2 calculations are presented for January, as there is a relatively small seasonal dependence; for ozone, where seasonal variations larger, results are presented as annual-means derived from monthly-mean calculations.

Table 3 (and Figure 1) shows the forcing for CO_2 increasing from 278 to 417 ppm; the IRF_{SW} is +5.6% of IRF_{NET} at TOA and −5.2% at the tropopause, consistent with earlier literature (Section 2). The effect of stratospheric temperature adjustment on RF_{NET} is much larger at TOA (increasing it by 70%) than at the tropopause (decreasing it by 8%), consistent with earlier literature. This means that RF_{SW} (which is unchanged from IRF_{SW} because of the weak impact of stratospheric temperature change) is a smaller component of RF_{NET} at TOA (3.3%) and a slightly larger tropopause component (−5.6%). As required, RF_{NET} now agrees at TOA and tropopause but, as shown in Table 3 and Figure 1 (left), the apparent SW attribution differs in sign between these levels.

However, this does not account for the role of SW absorption in temperature adjustment. This can be assessed by calculating RF_{NET} due to LW processes alone (Etminan et al., 2016; Myhre et al., 1998). The lower two rows in Table 3 shows this LW-only RF_{NET} is 0.05 $W \cdot m^{-2}$ greater than the full RF_{NET}. This 0.05 $W \cdot m^{-2}$ reduction in RF_{NET} robustly indicates the

TABLE 3 Global-mean instantaneous and adjusted radiative forcing ($W \cdot m^{-2}$) for January at the top-of-atmosphere and tropopause for an increase in CO_2 from 278 to 417 ppm

	Instantaneous			Adjusted		
$W \cdot m^{-2}$	LW	SW	Net	LW	SW	Net
TOA	+1.18	+0.07	+1.25	+2.07	+0.07	+2.14
Tropopause	+2.44	−0.12	+2.32	+2.26	−0.12	+2.14
TOA LW only (SW impact)	+1.18	0.0	+1.18	+2.19 (−0.12)	0.0 (+0.07)	+2.19 (−0.05)
Tropopause LW only (SW impact)	+2.44	0.0	+2.44	+2.19 (+0.07)	0.0 (−0.12)	+2.19 (−0.05)

Note: The third and fourth rows show the case for LW-only calculations. The values in parentheses are the component of the full LW + SW forcing that is attributed to SW forcing; these are derived by differencing row 1 from row 3 for TOA and row 2 from row 4 for the tropopause.

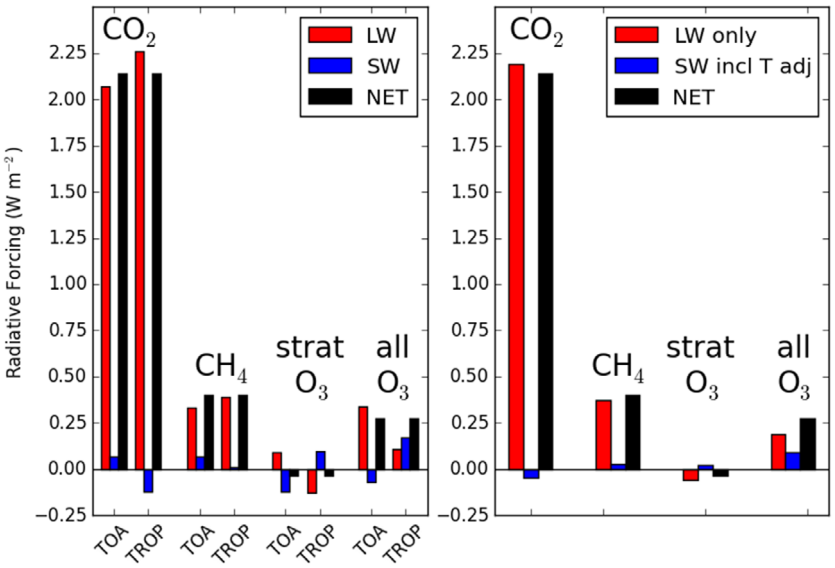

FIGURE 1 (left) radiative forcing (in $W \cdot m^{-2}$) at the top-of-atmosphere (TOA) and tropopause (TROP) separated into longwave, shortwave and net forcing, for the CO_2 and CH_4, and stratospheric and whole atmosphere O_3 perturbations described in the text. (right) radiative forcing separated into longwave, shortwave and net forcing when the component of LW forcing due to temperature adjustment resulting from the SW forcing is attributed to the SW forcing. In this case, TOA and TROP forcings are identical

TABLE 4 Global-mean instantaneous and adjusted radiative forcing ($W \cdot m^{-2}$) for January at the top-of-atmosphere and tropopause for an increase in CH_4 from 725 to 1450 ppb

	Instantaneous			Adjusted		
$W \cdot m^{-2}$	LW	SW	Net	LW	SW	Net
TOA	+0.37	+0.07	+0.44	+0.33	+0.07	+0.40
Tropopause	+0.36	+0.01	+0.37	+0.39	+0.01	+0.40
TOA LW only (SW impact)	+0.37	0.0	+0.37	+0.37 (−0.04)	0.0 (+0.07)	+0.37 (+0.03)
Tropopause LW only (SW impact)	+0.37	0.0	+0.37	+0.37 (+0.02)	0.0 (+0.01)	+0.37 (+0.03)

Note: The third and fourth rows show the case for LW-only calculations. The values in parentheses are then the component of the full LW + SW forcing that is attributed to SW forcing.

total impact of SW forcing, accounting for the direct effect via IRF_{SW}, and its indirect impact on RF_{LW} via stratospheric temperature change. RF_{NET} decreases by 2.3% at both TOA and tropopause (see Figure 1 [right]). As in Section 2, the contribution of the direct IRF_{SW}, and its impact on RF_{LW}, differs depending on TOA and tropopause perspectives. In this case the positive TOA IRF_{SW} gives an incorrect perception of the sign of SW absorption. Tropopause IRF_{SW} significantly overemphasises the size of the (negative) SW forcing, as noted by Myhre et al. (1998).

In the Section 3 idealised calculations, the RF_{LW} due to SW absorption was approximately equal and opposite at TOA and tropopause. For CO_2, the additional SW absorption is mostly in the upper stratosphere; the effect on RF_{LW} is about 1.7 times higher at TOA than at the

TABLE 5 Annual-mean global-mean instantaneous and adjusted radiative forcing ($W \cdot m^{-2}$) at the top-of-atmosphere and tropopause for the stratospheric ozone perturbation described in the text

	Instantaneous			Adjusted		
$W \cdot m^{-2}$	LW	SW	Net	LW	SW	Net
TOA	−0.045	−0.121	−0.166	+0.088	−0.121	−0.033
Tropopause	−0.021	+0.094	+0.072	−0.128	+0.095	−0.033
TOA LW only (SW impact)	−0.045	0.0	−0.045	−0.057 (+0.145)	0.0 (−0.121)	−0.057 (+0.024)
Tropopause LW only (SW impact)	−0.021	0.0	−0.021	−0.057 (−0.071)	0.0 (+0.095)	−0.057 (+0.024)

Note: The third and fourth rows show the case for LW-only calculations. The values in parentheses are then the component of the full LW + SW forcing that is attributed to SW forcing.

TABLE 6 As Table 5, but for the ozone perturbation in the stratosphere and troposphere described in the text

	Instantaneous			Adjusted		
$W \cdot m^{-2}$	LW	SW	Net	LW	SW	Net
TOA	+0.08	−0.07	+0.01	+0.34	−0.07	+0.28
Tropopause	+0.31	+0.17	+0.47	+0.11	+0.17	+0.28
TOA LW only (SW impact)	+0.08	0.0	+0.08	+0.19 (+0.16)	0.0 (−0.07)	+0.19 (+0.09)
Tropopause LW only (SW impact)	+0.31	0.0	+0.31	+0.19 (−0.08)	0.0 (+0.17)	+0.19 (+0.09)

tropopause (compare the −0.12 and 0.07 $W \cdot m^{-2}$ values in parentheses in the adjusted RF_{LW} column of Table 3).

Table 4 and Figure 1 show results for methane doubling from 725 ppb. We will show elsewhere that the low spectral-resolution version of SOCRATES underestimates methane's IRF_{SW}; the purpose here is to illustrate processes, rather than to present definitive values for methane RF. In this case, both TOA and tropopause IRF_{SW} are positive, although TOA IRF_{SW} is more strongly so. Stratospheric temperature adjustment is small in the LW-only case (Etminan et al., 2016); both IRF_{NET} and RF_{NET} are 0.37 $W \cdot m^{-2}$. When SW is included, convergence of SW radiation in the stratosphere (0.06 $W \cdot m^{-2}$) drives a larger adjustment; IRF_{NET} and RF_{NET} differ by about 0.03 W m^{-2} at TOA and tropopause. Unlike the CO_2 case this is not sufficiently strong to reverse the sign of TOA RF_{SW} (it decreases from +0.07 to +0.03 $W \cdot m^{-2}$) but it significantly enhances tropopause RF_{NET} (from 0.01 to 0.03 $W \cdot m^{-2}$) compared to the IRF_{SW}, consistent with Etminan et al. (2016).

Figure 1 shows results for ozone perturbations, taking the CMIP6 case from Checa-Garcia et al. (2018) for stratospheric ozone change (Table 5) and stratospheric and tropospheric ozone change (Table 6) derived from multimodel averages. Forcing is calculated using decadal-mean ozone fields for 2000–2009, relative to 1850–1859.

Ozone differs from CO_2 and CH_4 because of the perturbation's more complex morphology, and because SW forcing plays a larger relative role (Figure 1). For stratospheric ozone depletion (Table 5) IRF_{SW} is negative at TOA (the decreased stratospheric absorption means more SW radiation is reflected). and positive at the tropopause (more radiation is transmitted through the stratosphere). In both cases IRF_{LW} is negative. The instantaneous divergence of forcing across the stratosphere (≈0.07 $W \cdot m^{-2}$ due to IRF_{LW} and ≈0.22 $W \cdot m^{-2}$ due to IRF_{SW}) drives strong stratospheric cooling. The reduced emission increases TOA RF_{LW} relative to IRF_{LW}, changing its sign from −0.045 to +0.088 $W \cdot m^{-2}$, and makes tropopause RF_{LW} more negative (−0.02 to −0.13 $W \cdot m^{-2}$). This reduces TOA RF_{NET} and changes the sign of tropopause RF_{NET}. Importantly, even though RF_{NET} is identical at TOA and tropopause, the LW and SW components are of opposite signs, explaining the apparent discrepancy mentioned by Michou et al. (2020) (see Section 2). The TOA RF is most consistent with the ERF perspective.

By comparing with the LW-only case, Table 5 and Figure 1 show the major effect of SW-induced stratospheric cooling on RF_{LW}. Without SW-induced cooling, RF_{LW} is −0.06 $W \cdot m^{-2}$ at TOA and tropopause; with it, they are +0.09 and −0.13 $W \cdot m^{-2}$ respectively.

The case with decreasing stratospheric and increasing tropospheric ozone (Table 6, Figure 1) is more complex than the stratosphere-only case. The biggest difference is the positive IRF_{LW} at both TOA and tropopause, but IRF_{SW} is also impacted via reduced SW reflection from the troposphere. The instantaneous divergence of forcing

across the stratosphere (0.23 $W \cdot m^{-2}$ due to LW and 0.24 $W \cdot m^{-2}$ due to SW) still drives strong stratospheric cooling. The SW forcing, via its impact on stratospheric temperature, increases TOA RF_{LW} by 85% (from 0.19 to 0.34 $W \cdot m^{-2}$) and decreases tropopause RF_{LW} by 45% (from 0.19 to 0.11 $W \cdot m^{-2}$). Unlike Table 5, RF_{LW} is positive at tropopause and TOA for both the full and LW-only case, as the forcing from tropospheric ozone increases dominates. As shown in Figure 1 (right), RF_{LW} is the dominant contributor to RF_{NET}, even when the impact of SW forcing on RF_{LW} is accounted for.

5 | CONCLUSIONS

Via idealised and more realistic calculations, the nature of SW radiative forcing has been investigated. It has been shown that even the sign of the SW forcing can differ between top-of-atmosphere and tropopause perspectives, even though, following stratospheric temperature adjustment, the net top-of-atmosphere and tropopause forcings are identical. This indicates that, on its own, the shortwave forcing is not a consistent indicator of its importance in net forcing.

A more consistent view is achieved by considering the impact of SW forcing on LW forcing via stratospheric temperature adjustment. This separation can be achieved by comparing calculations that include and exclude SW forcing.

In this perspective, not only do the top-of-atmosphere and tropopause perspectives agree in the net forcing, but also the partitioning between SW and LW agrees. In the specific case of increased CO_2, SW processes decrease the net forcing at both the top of the atmosphere and tropopause by 2.3%; this resolves an apparent contradiction in the earlier literature that indicated that the sign of the SW forcing differs between these perspectives. For methane, the instantaneous SW tropopause forcing is smaller than the top-of-atmosphere because it is a residual of negative forcing due to increased stratospheric absorption and positive forcing due to decreased tropospheric reflection; including the effect of this SW absorption on stratospheric temperatures achieves a more nuanced but consistent view. For the ozone, again the top-of-atmosphere and tropopause views of the importance of SW and LW components differ significantly unless the SW influence on LW forcing is accounted for.

The most important conclusion here is that in both radiative forcing and effective radiative forcing frameworks, the role of SW forcing, when it arises from atmospheric absorption (rather than scattering), cannot be assessed by considering changes in SW irradiances alone; indeed, even the implied sign of the SW forcing may be incorrect. We have demonstrated that this is the case for stratospheric temperature adjustment. More detailed calculations with ESMs would be needed to understand how other LW rapid adjustments are affected by SW forcings to achieve a more complete view.

AUTHOR CONTRIBUTIONS

Keith Shine: Conceptualization; formal analysis; investigation; methodology; supervision; visualization; writing – original draft; writing – review and editing. **Rachael Byrom:** Investigation; methodology; writing – original draft; writing – review and editing. **Ramiro Checa-Garcia:** Investigation; methodology; software; writing – original draft; writing – review and editing.

FUNDING INFORMATION

Rachael E. Byrom was supported by a PhD studentship funded via the UK Natural Environment Research Council Scenario Doctoral Training Partnership (Grant Number NE/L002566/1)

ORCID

Keith P. Shine https://orcid.org/0000-0003-2672-9978
Rachael E. Byrom https://orcid.org/0000-0002-5992-6962
Ramiro Checa-Garcia https://orcid.org/0000-0001-7653-3653

REFERENCES

Cess, R.D., Zhang, M.H., Potter, G.L., Barker, H.W., Colman, R.A., Dazlich, D.A. et al. (1993) Uncertainties in carbon-dioxide radiative forcing in atmospheric general-circulation models. *Science*, 262, 1252–1255. https://doi.org/10.1126/science.262.5137.1252

Chagas, J., Newnham, D., Smith, K. & Shine, K.P. (2001) Effects of improvements in near-infrared water vapour line intensities on short-wave atmospheric absorption. *Geophysical Research Letters*, 28, 2401–2404. https://doi.org/10.1029/2001GL012412

Checa-Garcia, R., Hegglin, M.I., Kinnison, D., Plummer, D.A. & Shine, K.P. (2018) Historical tropospheric and stratospheric ozone radiative forcing using the CMIP6 database. *Geophysical Research Letters*, 45, 3264–3273. https://doi.org/10.1002/2017gl076770

Collins, W.D., Feldman, D.R., Kuo, C. & Nguyen, N.H. (2018) Large regional shortwave forcing by anthropogenic methane informed by Jovian observations. *Science Advances*, 4, eaas9593. https://doi.org/10.1126/sciadv.aas9593

Collins, W.D., Ramaswamy, V., Schwarzkopf, M.D., Sun, Y., Portmann, R.W., Fu, Q. et al. (2006) Radiative forcing by well-mixed greenhouse gases: estimates from climate models in the Intergovernmental Panel on Climate Change (IPCC) fourth assessment report (AR4). *Journal of Geophysical Research-Atmospheres*, 111(D14), D14317. https://doi.org/10.1029/2005JD006713

Donohoe, A., Armour, K.C., Pendergrass, A.G. & Battisti, D.S. (2014) Shortwave and longwave radiative contributions to global warming under increasing CO_2. *Proceedings of the National Academy of Sciences of the United States of America*, 111, 16700–16705. https://doi.org/10.1073/pnas.1412190111

Dufresne, J.-L., Eymet, V., Crevoisier, C. & Grandpeix, J.-Y. (2020) Greenhouse effect: the relative contributions of emission height

and total absorption. *Journal of Climate*, 33, 3827–3844. https://doi.org/10.1175/jcli-d-19-0193.1

Etminan, M., Myhre, G., Highwood, E.J. & Shine, K.P. (2016) Radiative forcing of carbon dioxide, methane, and nitrous oxide: a significant revision of the methane radiative forcing. *Geophysical Research Letters*, 43, 12614–12623. https://doi.org/10.1002/2016gl071930

Forster, P. & Shine, K. (2002) Assessing the climate impact of trends in stratospheric water vapor. *Geophysical Research Letters*, 29, 10-1–10-4. https://doi.org/10.1029/2001GL013909

Forster, P.M.D., Ponater, M. & Zhong, W.Y. (2001) Testing broadband radiation schemes for their ability to calculate the radiative forcing and temperature response to stratospheric water vapour and ozone changes. *Meteorologische Zeitschrift*, 10, 387–393. https://doi.org/10.1127/0941-2948/2001/0010-0387

Freckleton, R., Highwood, E., Shine, K., Wild, O., Law, K. & Sanderson, M. (1998) Greenhouse gas radiative forcing: effects of averaging and inhomogeneities in trace gas distribution. *Quarterly Journal of the Royal Meteorological Society*, 124, 2099–2127. https://doi.org/10.1256/smsqj.55013

Gordon, I.E., Rothman, L.S., Hill, C., Kochanov, R.V., Tan, Y., Bernath, P.F. et al. (2017) The HITRAN2016 molecular spectroscopic database. *Journal of Quantitative Spectroscopy & Radiative Transfer*, 203, 3–69. https://doi.org/10.1016/j.jqsrt.2017.06.038

Hansen, J., Johnson, D., Lacis, A., Lebedeff, S., Lee, P., Rind, D. et al. (1981) Climate impact of increasing atmospheric carbon-dioxide. *Science*, 213, 957–966. https://doi.org/10.1126/science.213.4511.957

Hauglustaine, D.A., Granier, C., Brasseur, G.P. & Megie, G. (1994) The importance of atmospheric chemistry in the calculation of radiative forcing on the climate system. *Journal of Geophysical Research-Atmospheres*, 99, 1173–1186. https://doi.org/10.1029/93jd02987

Manabe, S. & Wetherald, R.T. (1967) Thermal equilibrium of the atmosphere with a given distribution of relative humidity. *Journal of the Atmospheric Sciences*, 24, 241–259. https://doi.org/10.1175/1520-0469(1967)024<0241:TEOTAW>2.0.CO;2

Michou, M., Nabat, P., Saint-Martin, D., Bock, J., Decharme, B., Mallet, M. et al. (2020) Present-day and historical aerosol and ozone characteristics in CNRM CMIP6 simulations. *Journal of Advances in Modeling Earth Systems*, 12, e2019MS001816. https://doi.org/10.1029/2019MS001816

Myhre, G., Highwood, E., Shine, K. & Stordal, F. (1998) New estimates of radiative forcing due to well mixed greenhouse gases. *Geophysical Research Letters*, 25, 2715–2718. https://doi.org/10.1029/98GL01908

Myhre, G., Kvalevag, M., Radel, G., Cook, J., Shine, K.P., Clarke, H. et al. (2009) Intercomparison of radiative forcing calculations of stratospheric water vapour and contrails. *Meteorologische Zeitschrift*, 18, 585–596. https://doi.org/10.1127/0941-2948/2009/0411

Myhre, G., Nilsen, J.S., Gulstad, L., Shine, K.P., Rognerud, B. & Isaksen, I.S.A. (2007) Radiative forcing due to stratospheric water vapour from CH_4 oxidation. *Geophysical Research Letters*, 34, L01807. https://doi.org/10.1029/2006GL027472

Myhre, G., Shindell, D., Bréon, F.-M., Collins, W., Fuglestvedt, J., Huang, J. et al. (2013) In: Stocker, T.F., Qin, D., Plattner, G.-K., Tignor, M., Allen, S.K., Boschung, J. et al. (Eds.) *Anthropogenic and natural radiative forcing. Climate change 2013: the physical science basis. Contribution of Working Group I to the fifth assessment report of the Intergovernmental Panel on Climate Change*. Cambridge, England: Cambridge University Press, pp. 659–740.

Pincus, R., Buehler, S.A., Brath, M., Crevoisier, C., Jamil, O., Franklin Evans, K. et al. (2020) Benchmark calculations of radiative forcing by greenhouse gases. *Journal of Geophysical Research-Atmospheres*, 125, e2020JD033483. https://doi.org/10.1029/2020JD033483

Pincus, R., Mlawer, E.J., Oreopoulos, L., Ackerman, A.S., Baek, S., Brath, M. et al. (2015) Radiative flux and forcing parameterization error in aerosol-free clear skies. *Geophysical Research Letters*, 42, 5485–5492. https://doi.org/10.1002/2015GL064291

Ramaswamy, V. & Bowen, M.M. (1994) Effect of changes in radiatively active species upon the lower stratospheric temperatures. *Journal of Geophysical Research-Atmospheres*, 99, 18909–18921. https://doi.org/10.1029/94jd01310

Ramaswamy, V., Collins, W., Haywood, J., Lean, J., Mahowald, N., Myhre, G. et al. (2018) Radiative forcing of climate: the historical evolution of the radiative forcing concept, the forcing agents and their quantification, and applications. *Meteorological Monographs*, 59, 14.11–14.101. https://doi.org/10.1175/amsmonographs-d-19-0001.1

Ramaswamy, V., Schwarzkopf, M.D. & Shine, K.P. (1992) Radiative forcing of climate from halocarbon-induced global stratospheric ozone loss. *Nature*, 355, 810–812. https://doi.org/10.1038/355810a0

Shine, K.P. & Myhre, G. (2020) The spectral nature of stratospheric temperature adjustment and its application to halocarbon radiative forcing. *Journal of Advances in Modeling Earth Systems*, 12, e2019MS001951. https://doi.org/10.1029/2019ms001951

Skeie, R.B., Myhre, G., Hodnebrog, Ø., Cameron-Smith, P.J., Deushi, M., Hegglin, M.I. et al. (2020) Historical total ozone radiative forcing derived from CMIP6 simulations. *npj Climate and Atmospheric Science*, 3, 32. https://doi.org/10.1038/s41612-020-00131-0

Slingo, A. & Schrecker, H.M. (1982) On the shortwave radiative properties of stratiform water clouds. *Quarterly Journal of the Royal Meteorological Society*, 108, 407–426. https://doi.org/10.1002/qj.49710845607

Smith, C.J., Kramer, R.J., Myhre, G., Forster, P.M., Soden, B.J., Andrews, T. et al. (2018) Understanding rapid adjustments to diverse forcing agents. *Geophysical Research Letters*, 45, 12023–12031. https://doi.org/10.1029/2018GL079826

Walters, D., Baran, A.J., Boutle, I., Brooks, M., Earnshaw, P., Edwards, J. et al. (2019) The Met Office Unified Model global atmosphere 7.0/7.1 and JULES global land 7.0 configurations. *Geoscientific Model Development*, 12, 1909–1963. https://doi.org/10.5194/gmd-12-1909-2019

How to cite this article: Shine, K. P., Byrom, R. E., & Checa-Garcia, R. (2022). Separating the shortwave and longwave components of greenhouse gas radiative forcing. *Atmospheric Science Letters*, e1116. https://doi.org/10.1002/asl.1116